AERO-KINEMATIC OPTIMIZATION OF HIGH-LIFT DEVICES WITH DOWNWARD DEFLECTION OF SPOILER

Chuang Wei[1,2], Chong Rao[1,2], Long Yang[1,2] & Tiejun Zhang[1,2]

[1]AVIC Aerodynamics Research Institute, No.1 Yangshan Road, Shenyang, 110034, China
[2]Aero Science Key Lab of High Reynolds Aerodynamic Force at High Speed, No.1 Yangshan Road, Shenyang, 110034, China

Abstract

In this paper, based on aerodynamic optimization software named XunZhu developed by Aerodynamics Research Institute, Aero-Kinematic optimization of high-lift devices with downward deflection of spoilers was established. The surrogate-based optimization method was adopted, coupled with the parameterized module of high-lift devices mechanisms, the RBF mesh deformation method, and the high-confidence numerical simulation method to construct the objective function for the aerodynamic performance of multi-element airfoils at the typical section of wing, which was used to evaluate the aerodynamic performance of the high-lift device. The optimization cases show that the Pareto front satisfying the constraints is achieved, and the lift coefficients of design points 1 and 2 are greatly improved. Comparisons between the optimization named OPT2 and the Baseline of three-dimensional configuration, OPT2 configuration has larger lift, increase of lift coefficient at α=4° is 1.16%, and at maximum lift coefficient is 2.07%. The optimization design method of the high-lift devices subject to kinematic constraints developed in this paper is effective.

Keywords: high-lift device; kinematic mechanisms; optimization; surrogate-based optimization

1. Introduction

Commercial aircraft need high-lift systems during take-off and landing to generate enough lift at low speeds, and the design of the high-lift system is crucial for the success of a commercial aircraft. The significance of weight and aerodynamic performance of high-lift system in aircraft design is demonstrated by Meredith [1]. For example, an increase of 0.1 in lift coefficient at constant angle of attack results in a reduction of approach attitude by about one degree, reducing landing gear length and thereby saving up to 1400 lb. Moreover, an increase of 1.5% in maximum lift coefficient may result in an extra 6600 lb payload at fixed approach speed while a 1% increase in take-off lift over drag ratio (L/D) is equal to a 2800 lb increase in payload or a 150 nm range increase.

To improve the aerodynamic performance, numerical optimization method is widely applied in aerodynamic design optimizations of thigh-lift devices, however, most studies are mainly aimed at optimization of multi-element airfoil, while they are single disciplinary aerodynamic optimization, other constraints especially kinematic mechanisms constraints is not enough [2-6]. The aim of this work is to develop Aero-Kinematic optimization methodology, which used to design a high-lift system with improved aerodynamic performance and a realizable kinematic mechanism.

2. Optimization methodology

2.1 Design parameters

The aircraft wing leading edge is equipped with a Droop Nose Device (DND) inboard and slat outboard. At the trailing edge two Adaptive Dropped Hinge Flaps (ADHF) with downward deflection of spoilers are installed, which is sketched in Figure 1，the ADHF is characterized by a simple mechanism of a flap connected to a fixed hinge and pure rotational movement, which is mechanically simpler than a conventional Fowler flap and requires fewer moving parts, resulting in

a considerable reduction in weight. The position of the hinge rotation axis can be determined by using the coordinates of both the inner and outer ends of the rotation axis. Intuitively, these coordinates can directly be used as optimization variables. However, using the rotation point coordinates as the optimization variable frequently leads to incorrect lift device configurations, such as the main wing and flap intersecting.

The following methods have been adopted to solve the above problems. Take the flap inboard as an example, according to gaps and overlaps at inner and outer ends wing sections (such as C1 and C2 in Figure 1) and deflection of flap, the hinge rotation axis is obtained, and the kinematic mechanism of flap is determined. The typical wing section (such as sec1 in Figure 1) is chosen for aerodynamic performance evaluation. Eighteen design variables are defined in the optimization process:

(1) Deflection of DND inboard.

(2) Five setting parameters of slat outboard, including gaps and overlaps (left of Figure 2) at sections c3 and c5, deflection of slat outboard.

(3) Five settings parameters of flap inboard, including gaps and overlaps (right of Figure 2) at sections c1 and c2, deflection of flap inboard..

(4) Five settings parameters of flap outboard, including gaps and overlaps at sections c3 and c4, deflection of flap inboard.

(5) Two deflections of spoilers inboard and outboard.

The lower and upper bounds for design variables described above are summarized Table 2.

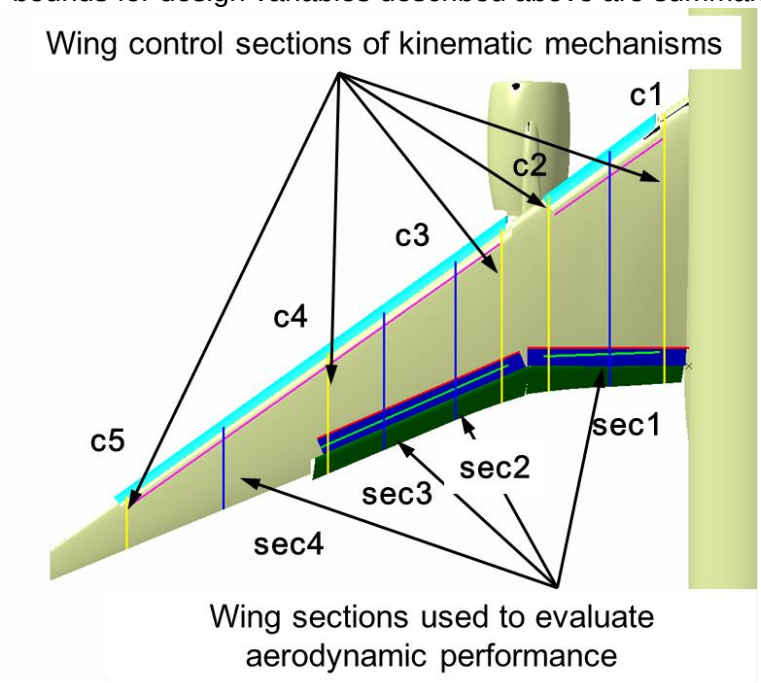

Figure 1 –Typical wing sections of kinematic mechanisms and used to evaluate the aerodynamic performance

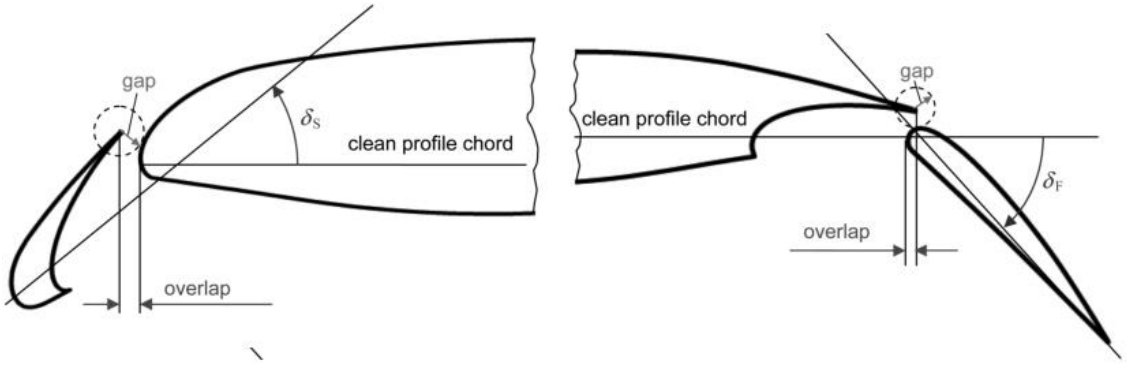

Figure 2 – Gap, overlap and Slat and deflection of flap parameterization [7]

Table 1 – List of design variables and ranges

NO.	Design variable	lower bound	upper bound
1	Deflection of DND inboard, deg	20	25
2	Deflection of spoiler inboard, deg	0	10
3	Deflection of ADHF inboard, deg	30	45
4	Gap ADHF of wing section C1	0.005	0.025
5	Overlap ADHF of wing section C1	0	0.01
6	Gap ADHF of wing section C2	0.005	0.025
7	Overlap ADHF of wing section C2	0	0.01
8	Deflection of slat outboard, deg	20	30
9	Gap slat outboard of wing section C3	0.01	0.03
10	Overlap slat outboard of wing section C3	-0.01	0.01
11	Gap slat outboard of wing section C5	0.01	0.03
12	Overlap slat outboard of wing section C5	-0.01	0.01
13	Deflection of spoiler outboard, deg	0	10
14	Deflection of ADHF outboard, deg	30	45
15	Gap ADHF of wing section C3	0.005	0.03
16	Overlap ADHF of wing section C3	0	0.015
17	Gap ADHF of wing section C4	0.005	0.03
18	Overlap ADHF of wing section C4	0	0.015

2.2 Optimization objectives and constraint

The objectives considered are to maximize lift coefficient at angles of attack of 4° and 18° at landing operations by searching for Kinematic setting parameters for both slat, flap and spoiler. The design sate is Ma=0.2 and Re=38.0×10^6 based on mean aerodynamic chord (MAC). The optimization problems were described as follows:

objective:

$$(1)Max: C_{L-DP1} = \left([C_L * \mathrm{c}]_{@Sec1} + [C_L * \mathrm{c}]_{@Sec2} + [C_L * \mathrm{c}]_{@Sec3} + [C_L * \mathrm{c}]_{@Sec4}\right)_{@\alpha=4^\circ} \Big/ 4 * c_A$$

$$(2)Max: C_{L-DP2} = \left([C_L * \mathrm{c}]_{@Sec1} + [C_L * \mathrm{c}]_{@Sec2} + [C_L * \mathrm{c}]_{@Sec3} + [C_L * \mathrm{c}]_{@Sec4}\right)_{@\alpha=18^\circ} \Big/ 4 * c_A \quad (1)$$

$$S.T. \quad (1)C_{L-DP1} \geq C_{L-DP1@Baseline}$$

$$(2)C_{L-DP2} \geq C_{L-DP2@Baseline}$$

2.3 Numerical method and validation

A two-dimensional incompressible Reynolds-Averaged Navier-Stokes (RANS) solver is utilized for computing the flow around multi-element airfoil configurations, and the turbulence model is k-ω SST model. A structured mesh was created and each airfoil element has a C-type mesh consists of 81000 cells (see Figure 3), it extends 40 chord lengths both upstream and downstream from the trailing edge of the main element. The normal mesh spacing at no-slip walls is 5×10^{-6} chord lengths to ensure y+<1. The lift curves and pressure coefficient distribution of the computational results are compared with the experimental data, as shown in Figure 4. It demonstrates that the lift coefficient and pressure coefficient distribution at α =16° is in good agreement with the experimental data. This shows that the present computational method is reliable.

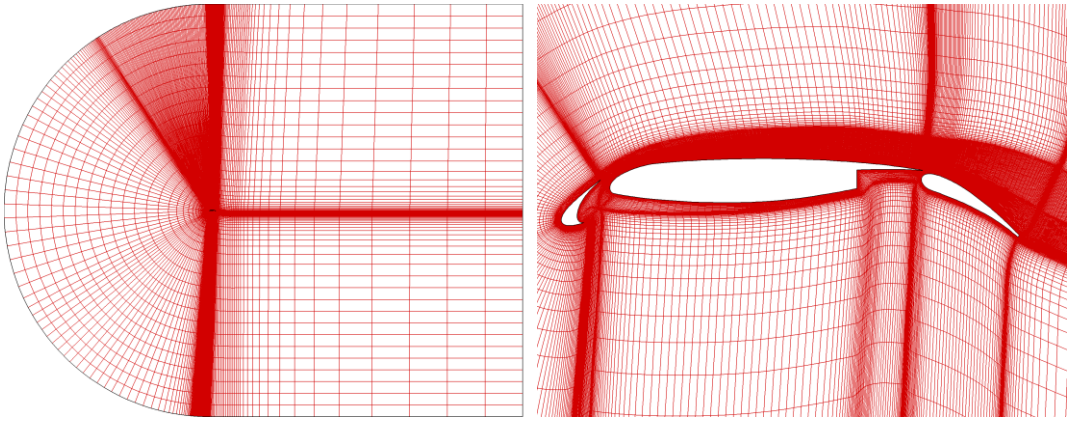

Figure 3 – The mesh of 30P30N multi-element airfoil

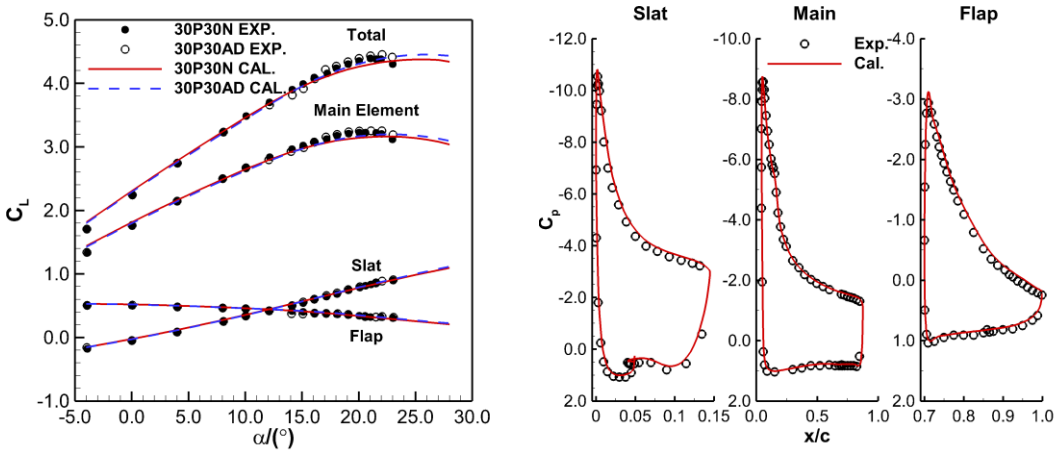

(a) C_L- α (b) C_p at α =16°

Figure 4 – Computational and experimental lift curves and pressure coefficient distribution

2.4 RBF mesh deformation method

A mesh deformation, based on radial basis functions (RBFs)[6], is devised in order to propagate the deformations from the boundaries to the interior of the CFD mesh. It creates new multi-element airfoil mesh based on the deformation of an initial mesh. The general solution for the deformation is given by

$$F(\mathbf{r}) = \sum_{i=1}^{N} \varpi_i \phi(\|\mathbf{r} - \mathbf{r_i}\|) \tag{2}$$

Where $F(\mathbf{r})$ is the function to be evaluated at location $\boldsymbol{r}$ and will define the motion of the volume points, i indicates the i th mesh nodes, N is the total number of mesh nodes, ϕ is the radial basis function. The coefficients ϖ_i are found by requiring exact recovery of the original function at these points $\mathbf{r_i}$.

In this paper, Wendland's C2 function was adopted for radial basis function, which has good computational efficiency and quality of mesh deformation. The initial and deformed meshes for multi-element airfoil are shown in Figure 5. The quality of the mesh deformation is higher, and the CPU time per deformed mesh which has nodes is less 1.0s.

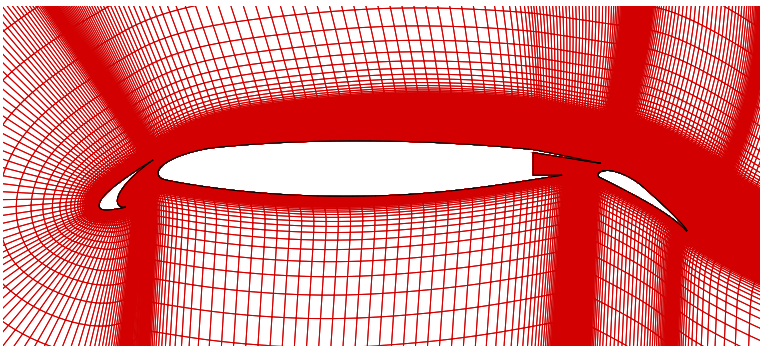

(a) Baseline mesh(δ_s=25°, δ_f=35°)

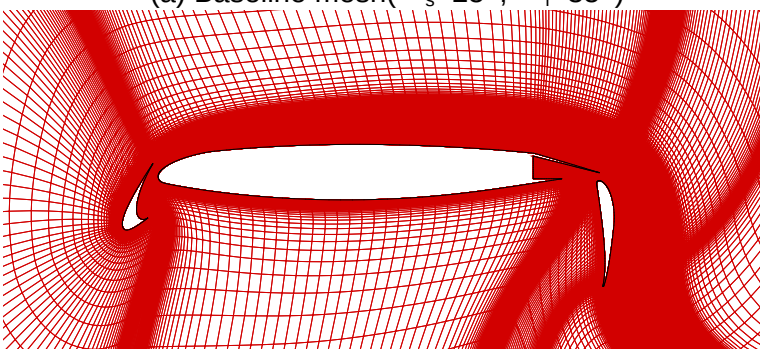

(b) Deformed mesh(δ_s=50°, δ_f=60°)

Figure 5 –Mesh deformation of multi-element airfoil configuration

2.5 Optimization process

Based on aerodynamic optimization software named XunZhu developed by Aerodynamics Research Institute [9], Aero-Kinematic optimization of high-lift devices with downward deflection of spoilers was established.The flow chart of aero-Kinematic optimization of high-lift devices is shown in Figure 6. The typical optimization process is as follows: (1) Initial sample points are chosen by design of experiments (DoE) method； response values are calculated by CFD solver and build the initial surrogate model. (2) Based on the surrogate model, the traditional optimization algorithm is used to solve the sub-optimization, and the new sample points are obtained according to infill-sampling criteria. (3) New sample points are evaluated by CFD added to the existing dataset, the surrogate model was constantly updated until global optimal solution is available.

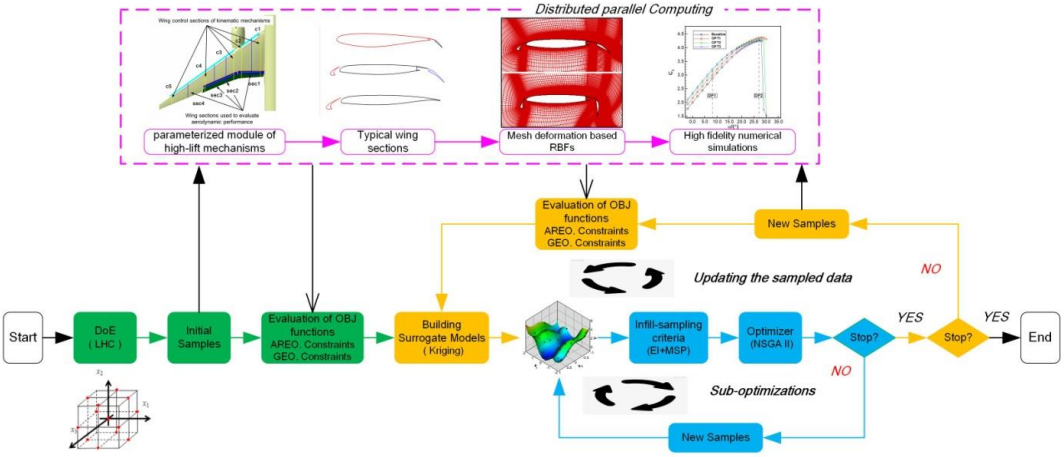

Figure 6 –Flow chart of Aero-Kinematic optimization of high-lift devices

3. Optimization results

The initial sample point is set to 108, the DoE method is Latin hypercube sampling (LHS), the surrogate model is Kriging, the infill-sampling criteria of minimizing surrogate prediction (MSP) for Pareto optimization was used to select 100 samples at each updating cycle and call 972 samples CFD evaluation in total. Figure 7 shows the final Pareto front, solutions named OPT1 and OPT3 are of primary importance, since they qualify the improvements in one objective while the other is kept fixed. From OPT1 to OPT3, the lift coefficient becomes larger and larger at α=4°, On the

other hand, the lift coefficient becomes smaller and smaller at the α =18º. OPT2 has larger lift both at α =4º and α =18º.

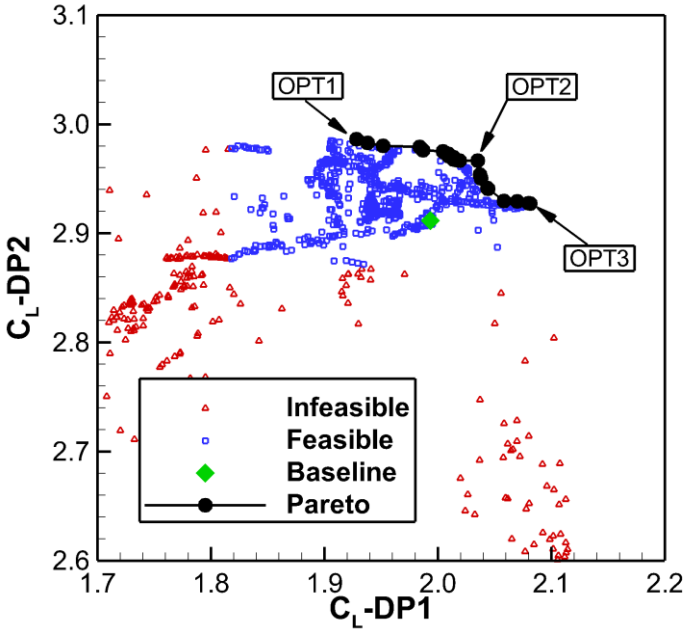

Figure 7 –Final Pareto front of optimization

Table 2 presents the set of Pareto optimal solutions, showing the values of the optimized design variables and comparing them with those of the baseline. The aerodynamic performances of the baseline and typical optimized configurations are listed in Table 3, which shows that the maximum increase of lift coefficient at α=4º is 4.40% (OPT3) and at α=18º is 2.56% (OPT1). Compare to baseline, OPT1 configuration has the largest maximum lift coefficient with a smaller increase at linear segment, while OPT3 configuration has the largest lift coefficient at linear segment with a smaller increase of maximum lift coefficient.

Table 2 –Pareto optimal design variable values for optimized solutions

NO.	Design variable	baseline	OPT1	OPT2	OPT3
1	Delta DND inboard, deg	22.00	23.69	24.94	24.92
2	Delta spoiler inboard, deg	5.00	10.00	10.00	9.99
3	Delta ADHF inboard, deg	40.00	38.73	34.75	34.21
4	Gap ADHF of C1	0.0060	0.0055	0.0052	0.0080
5	Overlap ADHF of C1	0.0080	0.0000	0.0001	0.0001
6	Gap ADHF of C2	0.0060	0.0053	0.0129	0.0129
7	Overlap ADHF of C2	0.0100	0.0100	0.0001	0.0003
8	Delta slat outboard, deg	25.00	20.01	20.01	20.00
9	Gap slat outboard of C3	0.0234	0.0225	0.0187	0.0188
10	Overlap slat outboard of C3	-0.0049	-0.0098	-0.0100	-0.0099
11	Gap slat outboard of C5	0.0205	0.0206	0.0293	0.0299
12	Overlap slat outboard of C5	-0.0021	-0.0078	-0.0089	-0.0067
13	Delta spoiler outboard, deg	5.00	10.00	10.00	9.99
14	Delta ADHF outboard, deg	40.00	41.14	44.46	44.36
15	Gap ADHF of C3	0.0100	0.0135	0.0083	0.0088
16	Overlap ADHF of C3	0.0120	0.0150	0.0148	0.0049
17	Gap ADHF of C4	0.0100	0.0050	0.0087	0.0089
18	Overlap ADHF of C4	0.0120	0.0102	0.0072	0.0071

Table 3 –Comparison of lift coefficient of baseline and optimal

Design points	4°	Δ $C_{L\text{-}DP1}$	18°	Δ $C_{L\text{-}DP1}$
baseline	1.9935		2.9117	
OPT1	1.9281	-3.28%	2.9862	2.56%
OPT2	2.0350	2.08%	2.9666	1.89%
OPT3	2.0812	4.40%	2.9274	0.54%

Comparison of DND, slat and flap settings among Baseline and OPT2 configuration is given in Figure 8. The lift coefficient curve among OPT2 and baseline of three-dimensional configuration is showed in Figure 9. Compare to baseline, OPT2 configuration has larger lift, increase of lift coefficient at $\alpha = 4^{o}$ is 1.16%, and at maximum lift coefficient is 2.07%.

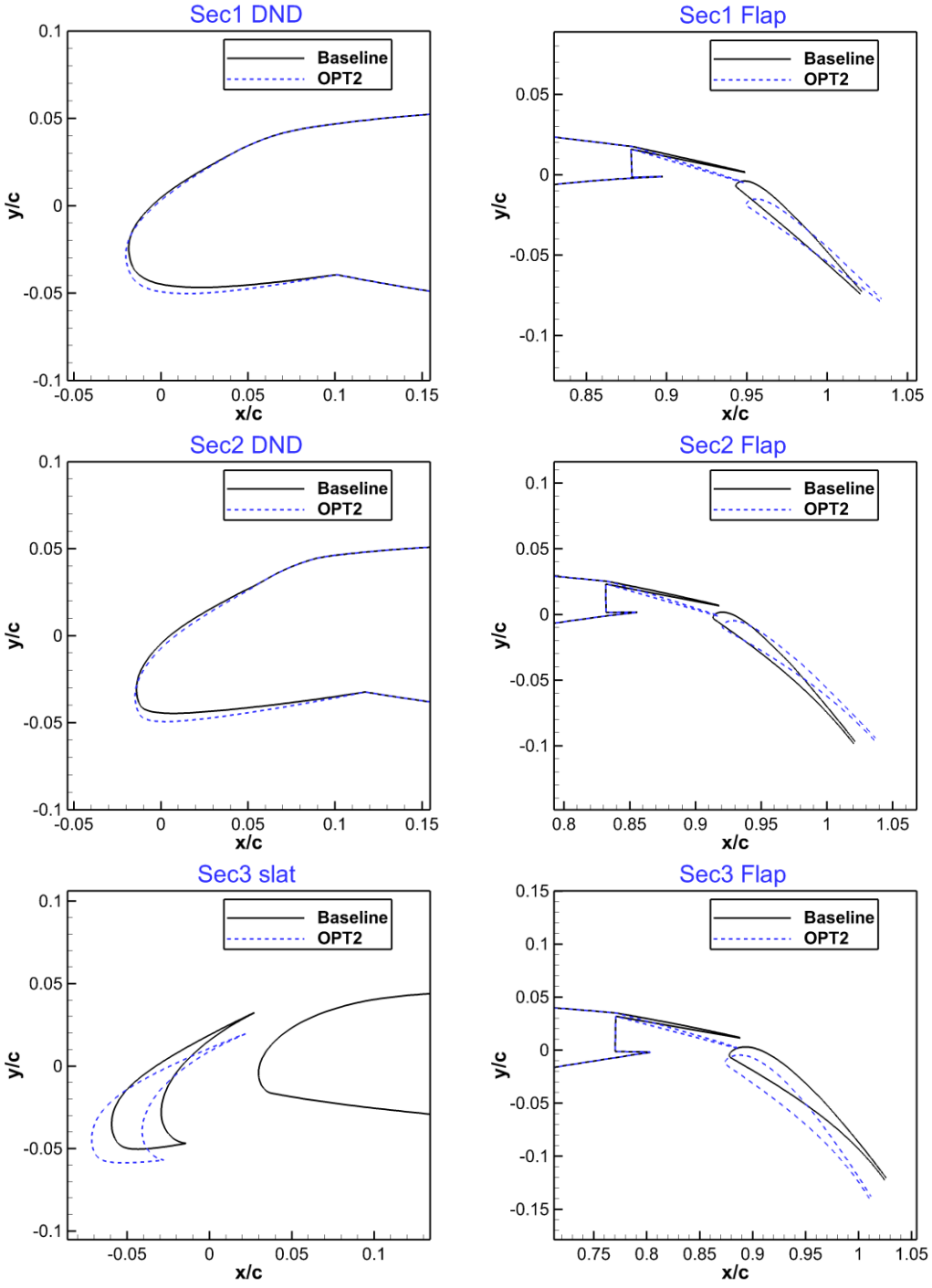

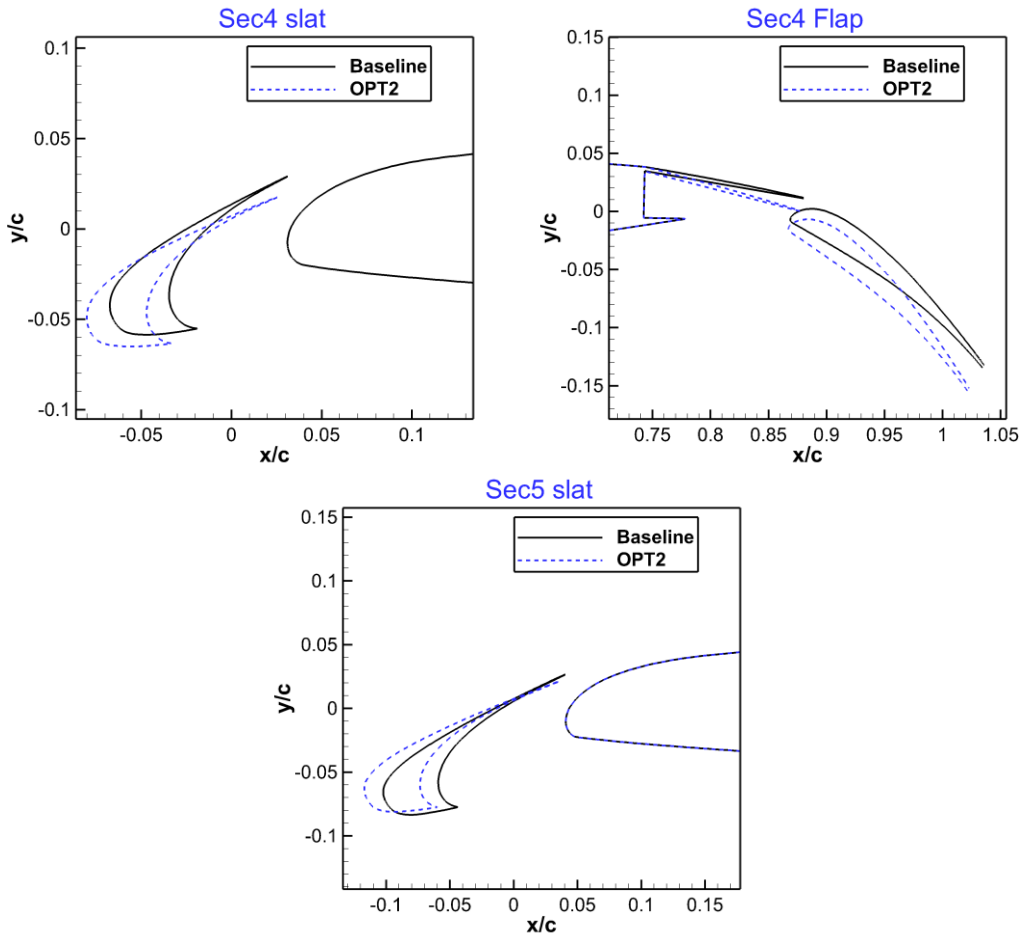

Figure 8 – Comparison of DND, slat and flap settings among Baseline and OPT2 configuration

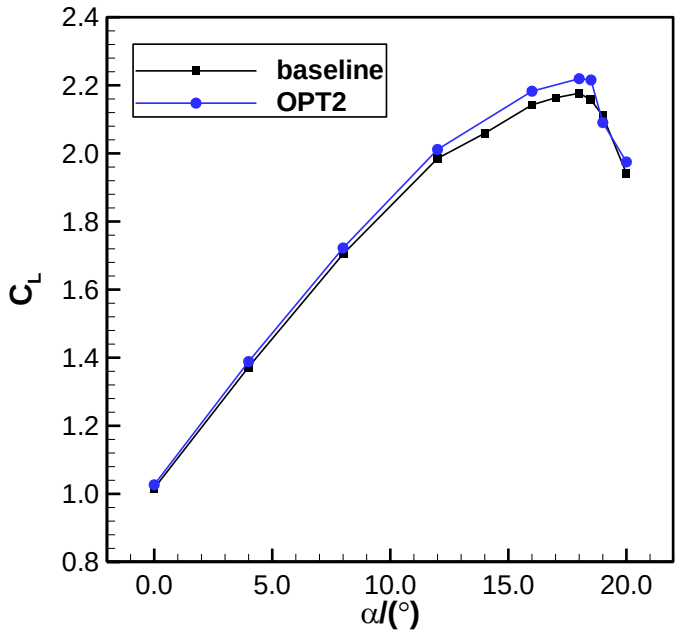

Figure 9 – Comparison of lift coefficient of baseline and OPT2 three-dimensional configuration

4. Conclusion

This paper summarizes the optimization design method of the high-lift devices subject to kinematic mechanism constraints. Comparisons between the optimization named OPT2 and the Baseline Comparisons between the optimization named OPT2 and the Baseline of three-dimensional configuration, OPT2 configuration has larger lift, increase of lift coefficient at α=4º is 1.16%, and at maximum lift coefficient is 2.07%. The objective to design a high-lift system with improved

aerodynamic performance was successfully achieved, which shows that the method is effective.

5. Contact Author Email Address

Chuang Wei: agangood@sina.com

6. Copyright Statement

References

[1] Meredith, P. T. "Viscous phenomena affecting high-life systems and suggestions for future CFD development." *High-Lift System Aerodynamics* (1993).

[2] Reckzeh, Daniel. "Multifunctional wing moveables: design of the A350XWB and the way to future concepts." *29th Congress of the International Council of the Aeronautical Sciences*. St. Petersburg: International Council of Aeronautical Sciences (ICAS), 2014.

[3] Strüber, Henning. "The aerodynamic design of the A350 XWB-900 high‐lift system." *29th international congress of the aeronautical sciences*. International Council of the Aeronautical Sciences (ICAS), 2014.

[4] Wang, Wenhu, Cyrille Breard, and Yifeng Sun. "Numerical study of the high-lift aerodynamic characteristics of dropped hinge flap coupled with drooped spoiler." *The Proceedings of the 2018 Asia-Pacific International Symposium on Aerospace Technology (APISAT 2018) 9th*. Springer Singapore, 2019.

[5] Dai, J. H., P. Q. Liu, and Ling Li. "Multi-Objective Aerodynamic Optimization of 2d High-Lift Device Based on Distributed Deep Reinforcement Learning." *33rd Congress of the International Council of the Aeronautical Sciences, ICAS, Stockholm*. 2022.

[6] Franke, Dirk M. "Aerodynamic optimization of a high-lift system with kinematic constraints." *New Results in Numerical and Experimental Fluid Mechanics VIII: Contributions to the 17th STAB/DGLR Symposium Berlin, Germany 2010*. Berlin, Heidelberg: Springer Berlin Heidelberg, 2013.

[7] Benini, Ernesto, Rita Ponza, and Andrea Massaro. "High-lift multi-element airfoil shape and setting optimization using multi-objective evolutionary algorithms." *Journal of Aircraft* 48.2 (2011): 683-696.

[8] De Boer, Aukje, Martijn S. Van der Schoot, and Hester Bijl. "Mesh deformation based on radial basis function interpolation." *Computers & structures* 85.11-14 (2007): 784-795.

[9] WEI C. YANG Long, LI Chunpeng, ZHANG Tiejun. “Research progress and application of ARI_OPT software for aerodynamic shape optimization.” *ACTA AERONAUTICAET ASTRONAUTICA SINICA*, 41-5(2020): 623370-623370